ACS Catalysis

Research Article

pubs.acs.org/acscatalysis

Unraveling the Catalytic Mechanism of Co_3O_4 for the Oxygen Evolution Reaction in a Li−O_2 Battery

Jinzhen Zhu,[†] Xiaodong Ren,[†] Jianjun Liu,*[,†] Wenqing Zhang,[†] and Zhaoyin Wen[‡]

[†]State Key Laboratory of High Performance Ceramics and Superfine Microstructure and [‡]CAS Key Laboratory of Materials for Energy Conversion, Shanghai Institute of Ceramics, Chinese Academy of Sciences, 1295 Dingxi Road, Shanghai 200050, People's Republic of China

Supporting Information

ABSTRACT: Unraveling the catalytic mechanism of transition-metal oxides (TMOs) for the charging reaction in a Li−O_2 battery and characterizing their surface structures and electronic structure properties of active sites are of great importance for the development of an effective catalyst to improve low round-trip efficiency and power density. In the current study, an interfacial model is first constructed to study the decomposition reaction mechanism of Li_2O_2 supported on Co_3O_4 surfaces. The computational results indicate that the O-rich Co_3O_4 (111)C with a relatively low surface energy in high O_2 concentration has a high catalytic activity in reducing overpotential and O_2 desorption barrier due to the electron transfer from the Li_2O_2 layer to the underlying surface. Meanwhile, the basic sites of Co_3O_4 (110)B surface induce Li_2O_2 decomposition into Li_2O and a dangling Co−O bond, which further leads to a high charging voltage in the subsequent cycles. The calculations for transition-metal (TM)-doped Co_3O_4 (111) indicate that P-type doping of Co_3O_4 (111) exhibits significant catalysis in decreasing both charging overpotential and O_2 desorption barrier. The ionization potential of doped TM is determined as an important parameter to regulate the catalytic activity of metal oxides.

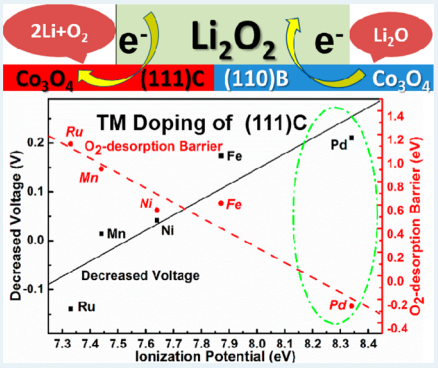

KEYWORDS: *lithium-O_2 battery, catalytic mechanism, Co_3O_4, doping transition metal, first-principles calculations*

1. INTRODUCTION

Rechargeable lithium−oxygen (Li−O_2) batteries have recently attracted great attention due to their superior energy storage density in comparison to conventional Li-ion batteries, which is critical to meet today's stringent power source requirements for electric vehicles and other high-energy applications.[1−7] However, the performance of Li−O_2 batteries is currently limited by several issues such as high charging overpotential,[8,9] low rate capability,[1,10,11] and poor cycling stability.[9,12,13] Nonaqueous aprotic Li−O_2 batteries are based on the net electrochemical reaction $2Li^+ + O_2 + 2e^- \leftrightarrow Li_2O_2$ with a thermodynamic potential of U_0 = 2.96 V from the Nernst equation. Many experiments determined modest discharging overpotential (~0.3 V) but very high charging overpotential (1.0−1.5 V), resulting in a low round-trip efficiency.[9,14−16]

Due to the limited polarization effects of lithium anodes, the large charging overpotential is mainly attributed to the sluggish oxygen evolution reaction (OER; $Li_2O_2 \rightarrow 2Li^+ + O_2 + 2e^-$) in an air electrode.[14,17,18] Tremendous research efforts in experiment and theory have been made to address this critical challenge by incorporating active catalysts in the cathode to enhance the kinetics of the OER: for example, metal oxides,[8,9,16,19−23] noble metals,[24−26] and ceramic based materials (TiN, TiC, and perovskites).[27−29] However, it is still controversial whether transition-metal oxides (TMOs) can improve the electrochemical performance of a Li−O_2 battery. Many TMOs were determined to have little, even no, catalytic effects in reducing overpotential and improving current density.[30] In contrast, some TMOs with novel nanostructures,[9,31] doping metals,[16] and conductive substrates[23,32,33] were experimentally found to have catalytic activity for the electrochemical reaction in a Li−O_2 battery. These differences stimulated us to elucidate what the key factor is in controlling the catalytic activity and designing a highly active catalyst. Therefore, unraveling the catalytic mechanism of TMOs and characterizing their structural and electronic properties related to catalytic activity are very important to develop practical devices with improved round-trip efficiency.

Among all applied metal oxides, the spinel Co_3O_4 with mixed oxidation states of Co^{2+} and Co^{3+} is promising, as it can significantly reduce OER overpotential and improve the cyclic performance of a Li−O_2 battery.[8] Previous studies showed that Co_3O_4 exhibited high catalytic activity in electrochemical water splitting,[34] Fischer−Tropsch synthesis,[35] and low-temperature CO oxidation.[36] After studying several metal oxides as cathode catalysts, Débart et al. found that Co_3O_4 supported on carbon gives the lowest charging voltage of ~4.0 V and maintains a relatively good discharging capacity.[8] In 2012, electrochemical studies on an innovatively designed Co_3O_4@Ni cathode demonstrated a higher rechargeable capacity and much lower

Received: June 4, 2014
Revised: November 11, 2014
Published: November 14, 2014

   dx.doi.org/10.1021/cs5014442 | ACS Catal. 2015, 5, 73−81

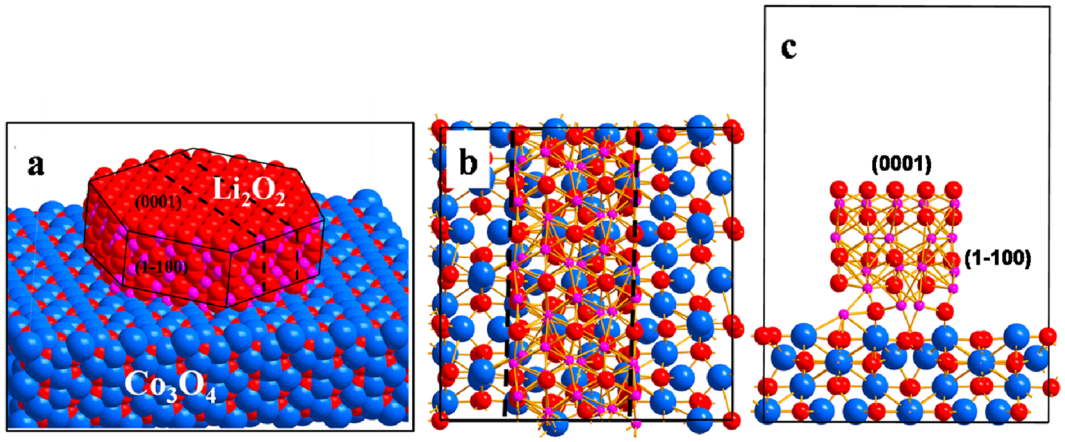

Figure 1. (a) Schematic diagram for the discharging product (Li_2O_2) deposited on the electrocatalyst surface (CO_3O_4). (b) Top and (c) side views of the computational model for the $Co_3O_4/Li_2O_2/O_2$ interface.

charging voltage (3.5 V) in comparison to noble metal Pt/Au as cathode catalyst.[14,23] However, the detailed catalytic mechanism is unclear. Very recently, Black et al. studied the electrochemical performance of Co_3O_4 grown on reduced graphene oxide (Co_3O_4@RGO) and observed kinetic improvement of mass transport for both the OER and the oxygen reduction reaction (ORR; $2Li^+ + O_2 + 2e^- \rightarrow Li_2O_2$).[37] However, the conventional catalytic effect originating from electron transfer was not found. It is significantly important to develop a proper catalytic model and elucidate the catalytic mechanism of Co_3O_4 for the OER in a Li−O_2 battery.

During charging, the possible processes related to the catalytic mechanism include interfacial interactions, mass transport, and electrochemical reactions. The experimental characterization of these mechanisms is challenging, as the charging reaction mainly occurs in the interface between the cathode and Li_2O_2.[38] Although there are several theoretical calculations on OER mechanisms and kinetics of pure Li_2O_2,[39−41] computational studies determining the mechanism of Li_2O_2 oxidation on a catalyst and unravelling possible catalytic effects have been very limited so far.

In this paper, first-principles studies on the catalytic mechanism of Co_3O_4 surfaces on the OER of Li_2O_2 in a Li−O_2 battery are presented. The goal is to find whether the catalytic effect exists in the charging process and what the key factor is that influences the catalytic effect. On the basis of previous experimental and theoretical studies, the interfacial model of $Li_2O_2/Co_3O_4/O_2$ is constructed to study the Li_2O_2 OER mechanism on different catalytic surfaces. Further, TM-doping calculations have been performed to screen the effective TMs in reducing the charging overpotential and O_2 desorption barrier. Three design rules for an OER catalyst in a Li−O_2 battery are therefore proposed on the basis of our mechanistic studies.

2. COMPUTATIONAL DETAILS

First-principles calculations in this work were conducted using density functional theory (DFT) with the generalized gradient approximation (GGA) for the exchange-correlation function as formulated by Perdew, Burke, and Ernzerhof (PBE). The valence electron−ion interaction was modeled by the projector augmented wave (PAW) potential as implemented in the Vienna ab initio simulation package (VASP).[42,43] A plane wave basis set with a cutoff energy of 450 eV was used. Electron correlation within the d states significantly affects the electronic structure and energetic properties of transition-metal oxides.[44,45] On the basis of the previous reports, the GGA+U (U = 2.0 eV) approach was used in our calculations.[45,46] The band gap of bulk Co_3O_4 is calculated to be 1.51 eV by DFT+U, which is consistent with the experimental value (1.44−1.52 eV).[47−50]

For the well-known overbinding issue of the O_2 molecule using DFT, the energy of the O_2 molecule is determined by the formula $H(T = 0\ \mathrm{K},O_2) = 2H(T = 0\ \mathrm{K},O) - \Delta E^{\mathrm{exptl}}$,[51] where $\Delta E^{\mathrm{exptl}}$ (5.12 eV) is the binding energy of O_2[52] and $H(T = 0, X)$ is the calculated ground state energy of the oxygen atom (X = O) or oxygen molecule (X = O_2). The free energy of O_2 includes the enthalpic contributions of 7/2 k_BT from transitional, rotational, and PV degrees of freedom, while the entropic contributions are taken from tabulated experimental data.[51,52] On the basis of experimentally thermodynamic data of bulk Li_2O_2 and Li,[52] the open-circuit potential of $2Li^+ + O_2 + 2e^- \leftrightarrow Li_2O_2$ is 2.98 V, which is close to the experimental value (2.96 V). The formation enthalpy and Gibbs energy of Li_2O_2 from calculations are −6.57 and −5.96 eV, respectively, which are in good agreement with the experimental data (−6.57 and −5.92 eV).[53]

In the charging process, Li^+ ions under an electromotive force are desorbed from the $Li_2O_2/Co_3O_4/O_2$ interface and subsequently diffused to the anode via the electrolyte.[39,54] Thermodynamically, the charging process can be described as

$$\Delta G = E - E_0 + \Delta N_{\mathrm{Li}}(\mu_{\mathrm{Li}} - eU) + \Delta N_{\mathrm{O_2}}\mu_{\mathrm{O_2}} \quad (1)$$

where E is the total energy of the slab, E_0 is the total energy of the initial slab, ΔN_{Li} and $\Delta N_{\mathrm{O_2}}$ are the numbers of Li and O_2 removed, and μ_{Li} and $\mu_{\mathrm{O_2}}$ represent the chemical potentials of Li bulk and O_2, respectively. U is the electromotive force corresponding to the charging voltage and can be derived from the thermodynamic equation of electrochemistry $\Delta G = \Delta G^0 + nFU$. The previous studies indicated that electrochemical process involving ion-coupled electron transfer can be well described by first-principles thermodynamics.[54] Although the same formula has been applied by different research groups to calculate the charging process of Li_2O_2, the definition of overpotential is different due to the shifting total free energy for each intermediate[39] or reaction step[40,41] to negative values. In this work, we define an overpotential by shifting the free

dx.doi.org/10.1021/cs5014442 | ACS Catal. 2015, 5, 73−81

energies of all intermediates to $\Delta G < 0$, which is consistent with ref 39.

3. RESULTS AND DISCUSSION

3.1. Interfacial Model of $Li_2O_2/Co_3O_4/O_2$. As discussed above, an effective computational model is important for accurately describing the catalytic mechanism of the OER in a Li−O_2 battery. There are two possible interfacial sites, cathode/Li_2O_2 and two-phase Li_2O_2/electrolyte, in the OER of a Li−O_2 battery. The recent study by in situ transmission electron microscopy (TEM) on the OER of Li_2O_2 on MWCNT revealed that the reaction preferentially occurs in the three-phase interface cathode/Li_2O_2/electrolyte rather than the two-phase interface electrolyte/Li_2O_2.[38] On the basis of these results, a theoretical model in which a nanoscale Li_2O_2 is deposited on Co_3O_4 surfaces to form a solid−solid interface was constructed, as shown in Figure 1a. Subsequently, Co_3O_4 surface structures and supported Li_2O_2 nanostructures should be described accurately on the basis of the previous experimental and theoretical data.[23,44,51]

The spinel Co_3O_4 exhibits rich surface-dependent catalysis due to different Co^{2+}/Co^{3+} percentages on specific surfaces.[44,45,55] Careful inspection of experimental data finds that Co_3O_4 (110) and (111) facets are exposed in a number of nanostructures.[56−58] The experimental studies on Co_3O_4@Ni by Cui et al. predicted that the Co_3O_4 (111) surface was likely to be exposed as the catalytic surface of the OER.[23] In addition, previous studies have demonstrated that Co_3O_4 (110) and (111) surfaces had high catalytic activity for the OER in electrochemical water-splitting cells.[34,59−61] In this work, the possible surface structures are determined by calculating their surface energies as a function of the chemical potential of oxygen. The calculated surface energies of Co_3O_4 (110), (111), and (311) facets correlating with the chemical potential of oxygen are presented in Figure S1 (Supporting Information). Under O-rich conditions, Co_3O_4 (111)C and (110)B have relatively low surface energies and are readily exposed with a large percentage area in the reaction of a lithium−air battery. The surface notations A−C in the present paper are labeled according to the traditional rule of discovered sequences in time. Co_3O_4 (110)B has been reported in previous literature, and Co_3O_4 (111)C is first found in the present work after the determined Co_3O_4 (111)A and (111)B.[44] The detailed structures of Co_3O_4 (110)B and (111)C are also illustrated in Figure S1. Due to their low surface energies, the Co_3O_4 $(1\bar{1}1)$C and (110)B surfaces were selected to explore the catalytic effect for the OER in a Li−O_2 battery. More importantly, the Co_3O_4 (111)C surface is fully oxygen terminated in a high O_2 pressure environment, while Co and O atoms coexist in the Co_3O_4 (110)B surface. The selection is aimed to determine the surface effects of catalytic activity for the OER in a Li−O_2 battery.

SEM observations indicated that the morphology of the discharging product Li_2O_2 exhibited toroidal and donutlike shapes.[62] Via calculating surface energies, Radin et al. established the equilibrium shape of Li_2O_2 with O-rich (0001) and $(1\bar{1}00)$ surfaces,[51] which was later confirmed by Yang et al.[63] Therefore, in our computational model, two O-rich surfaces ((0001) and $(1\bar{1}00)$) are exposed under vacuum to simulate the gas O_2 environment. Another dimension of Li_2O_2 is calculated periodically. Our calculations focus on the catalytic activity of different Co_3O_4 surfaces. A comparison of charging voltages in the different catalytic surfaces may cancel out the calculation error generated by the Li_2O_2 morphology when the same equilibrium structure of Li_2O_2 is used.

For a practical computational cost, the limited-size interfacial model of $Li_2O_2/Co_3O_4/O_2$ shown in Figure 1b,c has been constructed for calculations. The contact orientation of Li_2O_2 and Co_3O_4 is determined by the smallest lattice mismatch of Co_3O_4 and Li_2O_2 surfaces, which is shown in Figure S2 and Table S2 (Supporting Information). To build a stoichiometric structure, the Li layer of the Li_2O_2 surface is directly contacted with the Co_3O_4 surface while the O-rich surface of Li_2O_2 is exposed on the top layer, which is consistent with the computational results of Radin et al.[51] We further construct a Li_2O_2/Co_3O_4 interface model with a sandwich structure, as shown in Figure S3 (Supporting Information). Four layers of Co_3O_4 (110)B and five layers of Co_3O_4 (111)C are used in this model. After a structural relaxation, we found that the interfacial structure between Co_3O_4 and the first layer Li_2O_2 did not induce too much change in structure and charge distribution for the second layer Li_2O_2 (see Figure S4 (Supporting Information)). As a result, two layers of Li_2O_2 are deposited to interface with the Co_3O_4 surface and the top layer of Li_2O_2 is fixed in structural relaxations according to our trial calculations.

3.2. OER Mechanism of Li_2O_2 Supported on Co_3O_4 Surface. For comparison, OER paths starting from the Li_2O_2 $(1\bar{1}00)$ surface, which is directly exposed to vacuum in the $Li_2O_2/Co_3O_4/O_2$ interface,[51] were first calculated. The energy profile of stepwise Li^+ and O_2 desorption in OER paths is shown in Figure 2. Two possible reaction paths, $Li^+ \rightarrow Li^+ \rightarrow O_2$ and $Li^+ \rightarrow O_2 \rightarrow Li^+$, are considered on the basis of our previous calculations[64] and Ceder et al.'s work for Li_2O_2 oxidation.[39] In these reaction paths, O_2 desorption is the rate-determining step: 1.75 eV for $Li^+ \rightarrow Li^+ \rightarrow O_2$ and 3.33 eV for $Li^+ \rightarrow O_2 \rightarrow Li^+$. The charging voltage of the favorable path $Li^+ \rightarrow Li^+ \rightarrow O_2$ is calculated as 3.23 V, which is consistent with the calculated value (2.83 V) of Ceder et al.[39] after taking account of the difference in O_2 potentials (−9. 97 eV in their paper vs −9.12 eV in this work). Subsequently, these calculated

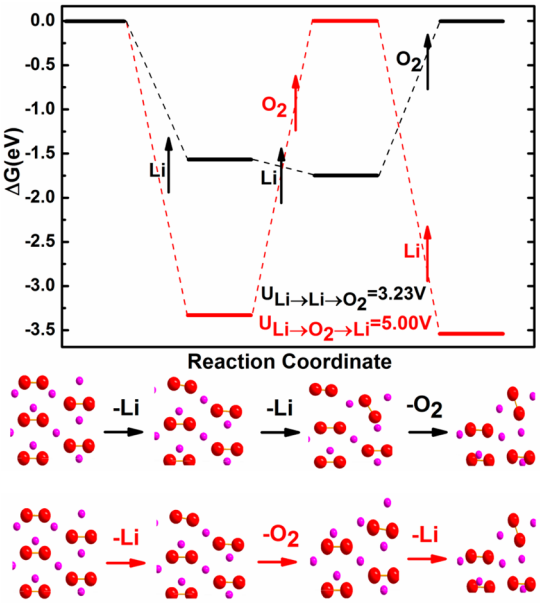

Figure 2. Energy profiles of possible OER paths starting from the Li_2O_2 $(1\bar{1}00)$ surface. The charging voltages for $Li^+ \rightarrow Li^+ \rightarrow O_2$ and $Li^+ \rightarrow O_2 \rightarrow Li^+$ are 3.23 and 5.00 V, respectively.

dx.doi.org/10.1021/cs5014442 | ACS Catal. 2015, 5, 73−81

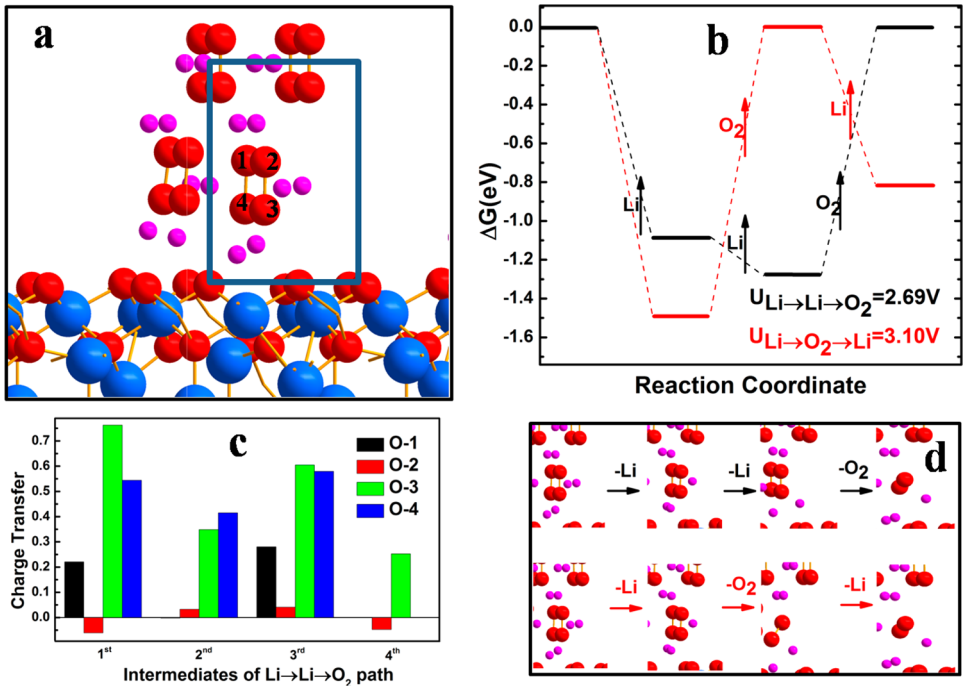

Figure 3. (a) Calculated structure of the Co_3O_4 (111)C/Li_2O_2/O_2 interface. The atoms in the rectanglular box are used to show structural evolution in (d). (b) Energy profiles of $Li^+ \rightarrow Li^+ \rightarrow O_2$ and $Li^+ \rightarrow O_2 \rightarrow Li^+$ OER paths of Li_2O_2. (c) Bader charge analysis of O1−O2−O3−O4 associated with the OER of Li_2O_2. The calculated O atoms in charge transfer analysis correspond to labeled O atoms in the box of (a). (d) Sketch map of $Li^+ \rightarrow Li^+ \rightarrow O_2$ and $Li^+ \rightarrow O_2 \rightarrow Li^+$ OER paths of Li_2O_2 (O2−O3).

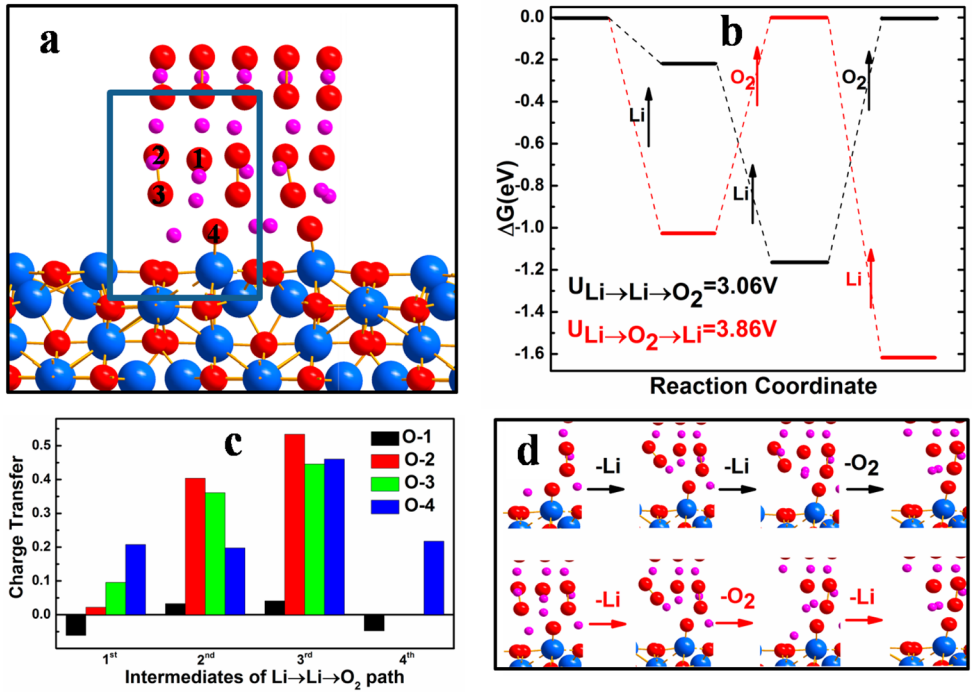

Figure 4. (a) Calculated structure of the Co_3O_4 (110)B/Li_2O_2/O_2 interface. The atoms in the rectanglular box are used to show structural evolution in (d). (b) Energy profiles of $Li^+ \rightarrow Li^+ \rightarrow O_2$ and $Li^+ \rightarrow O_2 \rightarrow Li^+$ OER paths of Li_2O_2. (c) Bader charge analysis of O1−O2−O3−O4 associated with the OER of Li_2O_2. The calculated O atoms in charge transfer analysis correspond to labeled O atoms in the box of (a). (d) Sketch map of $Li^+ \rightarrow Li^+ \rightarrow O_2$ and $Li^+ \rightarrow O_2 \rightarrow Li^+$ OER paths of Li_2O_2 (O2−O3).

charging voltages and O_2 desorption energies will be used as a reference to determine the catalytic activities of Co_3O_4 surfaces in the subsequent discussion.

On the basis of the established interfacial model, OER paths of the Li_2O_2-supported Co_3O_4 (111)C surface were calculated. A Bader charge analysis of the intermediates of the lowest-energy reaction path was performed to reveal the underlying catalytic mechanism. The calculated structure, energy profiles of OER paths ($Li^+ \rightarrow Li^+ \rightarrow O_2$ and $Li^+ \rightarrow O_2 \rightarrow Li^+$), and a charge analysis of OER intermediates of Li_2O_2 supported on

dx.doi.org/10.1021/cs5014442 | ACS Catal. 2015, 5, 73−81

Co_3O_4(111)C are given in Figure 3a−c, respectively. The structural evolutions of two reaction paths are shown in Figure 3d.

According to relaxed structures, we did not find any O−O bond cleavage of Li_2O_2 near the interface, but some Li^+ ions are attracted to approach the O-rich surface of Co_3O_4. In comparison, the O−O bond near the interface is 0.16 Å shorter than that of Li_2O_2 due to a large charge transfer from Li_2O_2 to the Co_3O_4 surface. The $Li^+ \rightarrow Li^+ \rightarrow O_2$ OER path corresponds to a relatively low charging voltage of 2.69 V, while the $Li^+ \rightarrow O_2 \rightarrow Li^+$ OER path requires a charging voltage of 3.10 V. In addition, the former requires overcoming a lower barrier (1.27 eV) of O_2 evolution, and the latter has a higher barrier of 1.50 eV for the corresponding step. A comparison with charging voltages of pure Li_2O_2 in Figure 2 reveals that the O-rich Co_3O_4 (111)C surface has a catalytic effect in reducing the overpotential of $\Delta U = 3.23 - 2.69 = 0.54$ V for the $Li^+ \rightarrow Li^+ \rightarrow O_2$ OER path and $\Delta U = 5.00 - 3.10 = 1.90$ V for the $Li^+ \rightarrow O_2 \rightarrow Li^+$ OER path. As shown in Figure 3c, both O2−O3 and O1−O4 have a significant electron transfer which enhances species conversion from O_2^{2-} to O_2.

There are two kinds of oxygen atoms on the Co_3O_4 (111)C surface: the two-coordinated (2c-O) and three-coordinated (3c-O) atoms. In the first step of the OER, the 2c-O and 3c-O gained 0.256 and 0.233 electron from high-energy occupied π^* orbitals of Li_2O_2, respectively. This electron transfer is favorable for Li_2O_2 desorption. Although 2c-O may have a slightly stronger ability to obtain electrons from Li_2O_2, the synergistic role of 2c-O and 3c-O in gaining electrons is expected to be more important. As a comparison, it is found that the Co−O coexistence surface will break the O−O bond of Li_2O_2, as indicated in the discussion of the Co_3O_4(110B) surface. Therefore, it is thought that a surface fully covered by electron acceptors may be significant for Li_2O_2 desorption.

Similarly, OER paths of Li_2O_2 supported on Co_3O_4 (110)B were calculated. The relaxed structure, energy profile of OER paths, Bader charge analysis for all intermediates, and structural evolutions of two OER paths are presented in Figure 4a−d, respectively. As shown in Figure 4a, a strong interfacial interaction between Li_2O_2 and Co_3O_4 induces O−O bond cleavage to form a dangling Co−O bond and Li_2O species due to electron transfer from the d orbital of Co to π^* of O_2. Particularly, this is an opposite electron transfer direction with Li_2O_2/Co_3O_4 (111)C. Therefore, two categories of Li_xO_y species, Li_2O_2 (O2−O3) and Li_2O (O1−O4), should be considered to unravel the OER mechanism.

First of all, we consider the OER mechanism of Li_2O_2 species on the Co_3O_4 (110)B surface. The calculated OER paths of Li_2O_2 (O2−O3) and corresponding structural evolution are presented in Figure 4b and d, respectively. The charging voltages for the $Li^+ \rightarrow Li^+ \rightarrow O_2$ and $Li^+ \rightarrow O_2 \rightarrow Li^+$ paths are calculated as 3.06 and 3.86 V, respectively. Taking pure Li_2O_2 (Figure 2) as a reference, we found that Co_3O_4 (110)B can decrease the charging overpotential with $\Delta U = 3.23 - 3.06 = 0.17$ V for the $Li^+ \rightarrow Li^+ \rightarrow O_2$ path and $\Delta U = 5.00 - 3.86 = 1.14$ V for the $Li^+ \rightarrow O_2 \rightarrow Li^+$ path. In addition, two rate-determining barriers of O_2 desorption steps are reduced to 1.15 eV in $Li^+ \rightarrow Li^+ \rightarrow O_2$ and 1.03 eV in $Li^+ \rightarrow O_2 \rightarrow Li^+$ in comparison with the O_2 desorption barriers of 1.75 and 3.33 eV in Figure 2. As a result, it is predicted that Co_3O_4 (110)B has a certain catalytic effect for Li_2O_2 species by reducing the charging overpotential and O_2 desorption barrier but this effect is weaker than that for Co_3O_4 (111)C. As shown in Figure 4c, O2−O3 in the second and third intermediates has a significant charge transfer which catalyzes Li_2O_2 oxidation and is favorable to O_2 desorption.

Previous experimental studies indicated that Li_2O might be formed with noble metals or metal oxides used as the cathode catalyst in a Li−O_2 battery.[3,30,65−68] However, the atomic scale OER mechanism for the Li_2O species is complicated and has not been fully established. Two possible OER mechanisms for Li_2O and O−Co* species are considered in the current calculations and are presented in the equations

$$Li_2O + O{-}Co* \rightarrow 2Li + O_2 + Co* \quad (3)$$

$$2Li_2O + 2O{-}Co* \rightarrow 4Li + O_2 + 2O{-}Co* \quad (4)$$

Equation 3 describes a continuous process of recombination of Li_2O and O(−Co) followed by desorption into O_2 and 2Li, refreshing the Co_3O_4 (110)B surface. The calculations show that this process requires a charging voltage of 5.61 V (see Figure S5 (Supporting Information)), which is unlikely to occur in practice. Equation 4 presents two formed Li_2O units combining together and desorbing into O_2 and 2Li, leaving O−Co bonds on the (110)B surface. The calculation obtained a charging voltage of 3.16 V, which is lower than the charging voltage (3.23 V) of Li_2O_2. These calculated results indicate that the possible discharging product Li_2O may decompose under catalysis of O-modified Co_3O_4 (110)B covering the Co atom with the O atom.

The calculations showed that O-modified Co_3O_4 (110)B covering the Co atom with the O atom may be generated in the first discharging process. Therefore, it is worth exploring the OER mechanism of Li_2O_2 supported on O-modified Co_3O_4 (110)B in order to determine its catalytic activity. The calculated energy profile of $Li^+ \rightarrow Li^+ \rightarrow O_2$ and optimized structures are presented in Figure 5. The charging voltage along

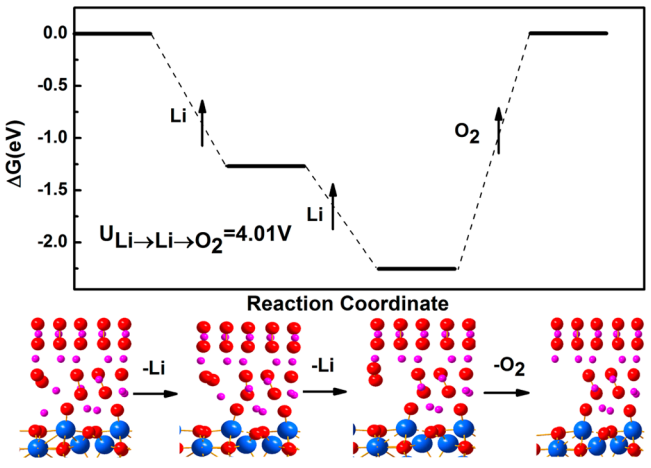

Figure 5. Calculated energy profiles of $Li^+ \rightarrow Li^+ \rightarrow O_2$ OER of Li_2O_2 supported on an O-modified Co_3O_4 (110)B surface.

this reaction path is calculated as 4.01 V, which is much higher than that (3.23 V) of clean Li_2O_2. A careful inspection of structures indicates that O(−Co) has a strong attraction for Li^+ ions. The Bader charge calculation shows that O(−Co) has an extra charge of $-1.6e^-$, indicating an electronic state of O^{2-}.

In summary, we predict that the Co/O-coexisted Co_3O_4 (110)B may reduce the charging overpotential by ~0.17 V and O_2 desorption barrier by ~0.60 eV in the first charging process. However, this catalytic activity in reducing charging voltage and

dx.doi.org/10.1021/cs5014442 | ACS Catal. 2015, 5, 73−81

Scheme 1. Comparison of Catalytic Mechanisms of Co_3O_4 (111)C and (110)B Surfaces for OER in Electrochemical Water Splitting and OER in a Li−O_2 Battery, Respectively[a]

(a) Interfacial OER of Li_2O_2 on O-rich Co_3O_4 (111)C Surface

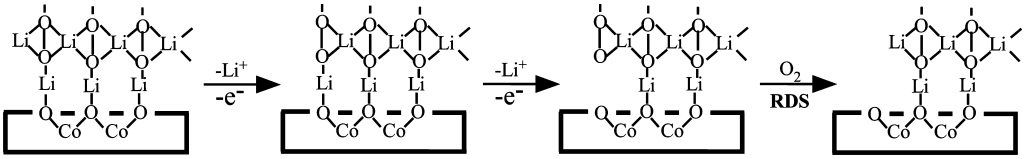

(b) Heterogeneous OER of H_2O on Co/O-coexisted Co_3O_4 (110)B Surface

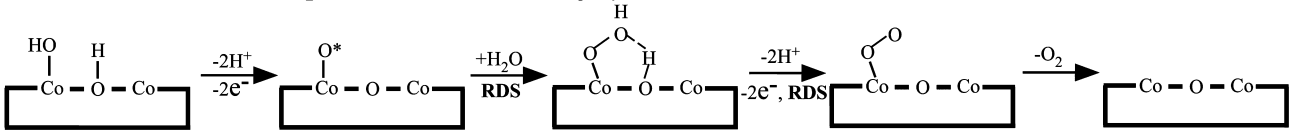

[a]Here, RDS represents the rate-determining step.

O_2 desorption energy may disappear in the subsequent cycles because the possible discharging product Li_2O has a relatively high charging voltage. Therefore, it is predicted that Co_3O_4 (110)B as a catalytic surface may have poor cycle performance in a Li−O_2 battery.

3.3. Influence of Surface Structure on Catalytic Activity. It is important to reveal surface effects of the catalytic activity on the basis of OER mechanisms of Li_2O_2 on Co_3O_4 (110)B and Co_3O_4 (111)C. According to the Bader charge analysis (Figures 3c and 4c), O-rich Co_3O_4 (111)C is determined to be a strong Lewis acid catalyst which prefers attracting electrons from Li_2O_2. Since such electron transfer enhances Li^+ and O_2 desorption, the charging voltage of Li_2O_2 is effectively decreased. In contrast, acidic sites (O sites) in the Co_3O_4 (110)B surface have a weak attraction for electrons in Li_2O_2, while basic sites (Co sites) of Co_3O_4 (110)B induce O−O bond cleavage to form a stable phase of Li_2O owing to electron transfer from Co atoms to Li_2O_2. The calculations suggest that the OER of Li_2O requires a relatively high charging voltage. Therefore, a catalytic surface with higher Lewis acidity corresponds to a higher catalytic activity for Li_2O_2 OER. It is concluded that an effective method to improve the catalytic activity of Li_2O_2 OER is to prepare a Lewis acid surface for transition-metal oxides at a high O_2 pressure.

On the basis of the calculated results, two strategies are proposed to improve the catalytic activity of the metal/oxygen-exposed surface. First of all, an effective passivation pretreatment for transition-metal sites under basic conditions is necessary to prevent reduction of Li_2O_2 to form Li_2O, which was confirmed by the recent experimental studies of Co_3Mo_3N and Ti/MnO_2 as bifunctional catalysts of the ORR and OER in a Li−O_2 battery.[19,69] Secondly, given the same surface structure, late-transition-metal oxides may have a higher catalytic activity for Li_2O_2 OER than early-transition-metal oxides due to the higher Lewis acidity.

Furthermore, the calculated OER mechanisms of a Li−O_2 battery on Co_3O_4 (111)C and electrochemical water splitting supported on Co_3O_4 (110)B[34] are compared. As shown in Scheme 1, the Co/O-coexisted Co_3O_4 (110)B surface was demonstrated to have high catalytic activity for water adsorption and the OER,[34] whereas the O-rich Co_3O_4 (111)C surface has no catalytic activity because O−H bonds cannot be broken without Co ions being involved.[70] The water adsorption and oxidation on Co_3O_4 surfaces are a typical of heterogeneous catalysis where molecular/atomic adsorption strength on the surface is of importance to determine catalytic activity. In contrast, different catalytic mechanisms of Co_3O_4 surfaces are presented in the OER of a Li−O_2 battery. The O-rich Co_3O_4 (111)C surface has a high catalytic activity for Li_2O_2 OER due to electron transfer from O_2^{2-} to the surface, while the Co/O-coexisted Co_3O_4 (110)B surface has a weak catalytic activity due to Li_2O formation. The Li_2O_2 decomposition on Co_3O_4 surfaces is interfacial catalysis between two solid phases. Therefore, long-range electron transfer play an important role in determining catalytic activity.

3.4. Tailoring Catalytic Activity by Doping TM. Effective surface enhancement such as TM doping has been extensively applied to improve the activities of catalysts.[71] Previous experimental studies showed that the introduction of a TM into metal oxides and nitrides could regulate the catalytic activity of the OER in a Li−O_2 battery.[16,19,69] Therefore, OER mechanisms of Li_2O_2 catalyzed by a TM-doped Co_3O_4 (111)C surface were calculated. In the present work, only TMs (Mn, Fe, Co, Ni, Ru, and Pd) nearby Co in the periodic table have been selected to substitute for Co. The Co atoms in the first layer are all three-coordinated with surrounding oxygen atoms. Three Co atoms are replaced by the selected TM corresponding to 25% doping concentration in the first layer. A relatively high doping concentration was designed so as to indicate an obvious catalytic effect. Moreover, the model is close to the real systems, as doping atoms will segregate to the surface, corresponding to a high doping concentration.[71] The detailed doping positions are illustrated in Figure S6 (Supporting Information). It should be pointed out that oxygen vacancies generated by doping different valence TMs were not considered in the current calculations. As reported by Metiu et al., oxygen vacancies with exposed TMs are strong bases that preferably donate electrons to Li_2O_2, which is unfavorable to the OER.[71,72]

In order to determine the thermodynamic stability of the doping system, the substituted energies have been calculated according to the equations

$$n\mathrm{M} + \mathrm{TMO}_{\mathrm{perfect}} \rightarrow \mathrm{TMO}_{\mathrm{doped}} + n\mathrm{Co} \quad (5)$$

$$E_S = \frac{E_{\mathrm{TMO\text{-}doped}} + nE_{\mathrm{Co}} - E_{\mathrm{TMO\text{-}perfect}} - nE_{\mathrm{M}}}{n} \quad (6)$$

dx.doi.org/10.1021/cs5014442 | ACS Catal. 2015, 5, 73−81

where M is the dopant and n is the number of M in the model per super cell. Co and M are both in the bulk phase. $E_{TMO\text{-}perfect}$ and $E_{TMO\text{-}doped}$ represent the total energies of clean and doped surfaces of TMO, respectively. According to the formula (6), the substituted energies of TM-doped Co_3O_4 (111)C (TM = Mn, Ni, Fe, Ru, Pd) were calculated as −1.99, 1.50, −0.46, −0.87, and −2.05 eV/atom, respectively. Except for Ni, other TMs have favorable thermodynamics to substitute for Co in Co_3O_4 (111)C.

The catalytic activities of TM-doepd Co_3O_4 were further established by calculating reducibility for overpotential and O_2 desorption barrier. The calculated values of decreased potential and O_2 desorption barrier were correlated with ionization potentials of doped transition metals. Figure 6 presents the

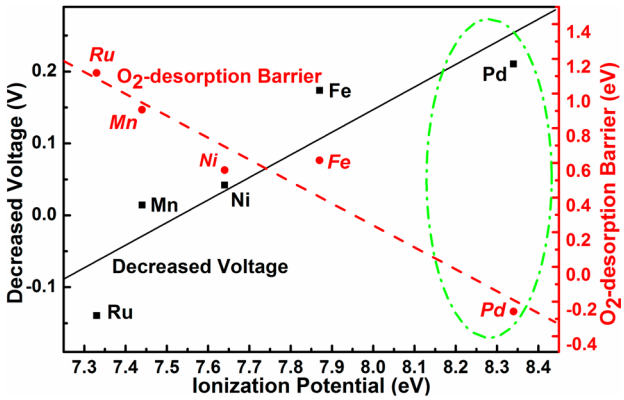

Figure 6. Decreased overpotential and O_2-desorption barrier in the OER of Li_2O_2 supported on TM-doped Co_3O_4 (111)C as a function of ionization potential of doped TM.

correlation of catalytic activity with ionization potential of doped TM. Pd-doped Co_3O_4(111) exhibited a comparable charging overpotential but exhibited a better catalytic activity in reducing O_2 desorption energy. Therefore, it is predicted to be a promising catalyst for the charging reaction of a Li−O_2 battery. While no Pd-doped Co_3O_4 as an OER catalyst has been reported so far, a similar system, Pd/MnO_2, was determined to have a higher current density and discharging capacity.[16] Future experimental studies of Pd-doped Co_3O_4 are highly desirable to confirm our prediction. In addition, Debart et al. found that $CoFe_2O_4$ had a weaker catalytic activity in reducing the overpotential and improving the discharging capacity,[8,14] which is qualitatively consistent with our calculations.

In fact, tuning the catalytic activity of Co_3O_4 (111) by doping TM is in nature consistent with the previously established structure−performance relation: that is, the Lewis acid strength of the catalyst surface is an important parameter to evaluate the catalytic activity for Li_2O_2 OER. In addition to preparing transition metal oxides under relatively high O_2 pressure, we further suggest another important strategy, doping TM with a higher ionization potential, to design catalysts for the Li_2O_2 OER.

3.5. Implication for Experiments. Our previous experimental studies showed that the overpotential at a low current density could be reduced by ∼0.6 V with Co_3O_4 catalyst in comparison to that with no catalyst.[14] This is in good agreement with our calculated results, in which the Co_3O_4 (111)C surface decreases the charging voltage by 0.54 V (3.23 − 2.69 V). In addition, Bruce et al. reported that Co_3O_4 on a carbon cathode could reduce the charging voltage by 0.5 V,[14] which is in qualitative agreement with our calculated value.

The present calculations reveal a possible mechanism of reducing overpotential by Co_3O_4, except for any complications of electrochemistry caused by electrolyte and electrode stability issues. There exists a great debate on the charging voltage of Li_2O_2 and the real effectiveness of electrocatalysis in a Li−O_2 battery. Experimental studies by Luntz et al. suggested that the charging plateau of Li_2O_2 should be ∼3.2 V and no OER catalysts were required.[30] However, they examined a Li−O_2 battery with a small capacity and a monolayer Li_2O_2 structure on a carbon electrode. Later, Yang et al. found that the charging voltage is apparently related to the size, composition, and morphology of discharging products.[73,74] The main charging plateau occurs at ∼3.4 V, corresponding to ∼0.5 V overpotential. According to first-principles thermodynamic calculations, Luntz et al. found a low OER overpotential in the various Li_2O_2 surfaces.[41] However, the OER takes place on the interface of the cathode and Li_2O_2 instead of the Li_2O_2 surface,[38] which may generate a higher overpotential. By using metal electrodes and stable electrolyte in a Li−O_2 cell, Bruce[28] and Wen[23] also found that charging voltages of Li_2O_2 should be 3.3−3.5 V without electrode and electrolyte stability issues. All this evidence indicates that only Li_2O_2 can usually generate the charging overpotential of 0.5 V, and electrocatalysis can reduce the charging overpotential ofa Li−O_2 battery. Such an overpotential may be ascribed to a slower electrochemical reaction (OER) but fast electron transport.[30,51] Therefore, our calculations focus on reducing the overpotential of 2.9−3.5 V, which originates purely from Li_2O_2 oxidation. The higher overpotential (3.5−4.0 V) observed in experiments may be interpreted as slow mass transport, desolvation, and side reactions.[30,75,76] Undoubtedly, it is relevant to reduce the OER overpotential of Li_2O_2, which can improve the round-trip efficiency of a Li−O_2 battery and avoid side reactions.

It is interesting to extend the calculated catalytic mechanism of Co_3O_4 to other TMOs as catalysts of the OER in a Li−O_2 battery. As indicated above, electron transfer from Li_2O_2 to the catalyst is the essence of catalytic activity in reducing charging overpotential and O_2 desorption energy. On the basis of our calculations, three rules are proposed for designing a novel catalyst. They are expected to provide guidance on possible ways to manipulate the surface structure of the catalyst. First of all, the higher the acidity of the surface structure of the catalyst, the higher the catalytic activity it has. Tuning the acidity of TMO surfaces has been elaborately discussed in a previous review.[71] A systematical study of TMOs to catalyze OER is underway in our group. Second, surface oxygen ions have strong Lewis acidity to attract electrons from Li_2O_2 and thus to enhance OER kinetics, whereas a basic surface with exposed Co leads to a highly stable Li_2O formation. It is predicted that TMOs with a higher O content on the surface may have a higher catalytic activity for Li_2O_2 OER because more Lewis acid sites could be exposed on their surfaces. Generally, TMOs prepared under a relatively high O_2 pressure have more O-exposed polar surface structures. Third, doping TM with a higher ionization potential in TMO is a very effective strategy to improve the catalytic performance of the OER in a Li−O_2 battery.

4. CONCLUSIONS

In the present paper, extensive DFT-based first-principles computational studies have been performed to understand the

dx.doi.org/10.1021/cs5014442 | ACS Catal. 2015, 5, 73−81

complicated OER mechanism of Li_2O_2 supported on Co_3O_4 surfaces. According to our calculated results, we conclude the following.

(1) On the basis of our calculations, we determined that the OER in a Li−O_2 battery should preferably occur in the Li_2O_2/catalyst/O_2 interface rather than the Li_2O_2 surface, which is consistent with experimental observations. The computational model of the OER mechanism should contain two solid phases and a vacuum.

(2) The Co_3O_4 (111)C surface with full coverage of Lewis acid sites has a high catalytic activity in reducing overpotential and O_2 desorption barrier due to electron transfer from Li_2O_2 to the catalytic surface. The basic sites of the Co_3O_4 (110)B surface induce Li_2O_2 decomposition into Li_2O and a dangling Co−O bond, which leads further to a high charging voltage in the subsequent cycles. This indicates that electron transfer from Li_2O_2 to the catalyst is favorable to reduce overpotential and O_2 desorption energy.

(3) The calculations for transition-metal (TM)-doped Co_3O_4 (111) indicate that P-type doping of Co_3O_4 (111) exhibits a good catalytic effect in decreasing both charging overpotential and O_2 desorption barrier. The ionization potential of doped TM has been determined to be an important parameter to regulate the catalytic activity of metal oxides.

(4) According to our calculated results, we propose three rules for designing an active catalyst to reduce overpotential and improve the current density of the OER in a Li−O_2 battery. Therefore, our mechanistic studies for the OER mechanism of Li_2O_2 supported on Co_3O_4 should be helpful in the development of a high-performance Li−O_2 battery.

■ ASSOCIATED CONTENT

Supporting Information

The following file is available free of charge on the ACS Publications website at DOI: 10.1021/cs5014442.

Surface energy curves of Co_3O_4, lattice mismatch calculations of different match models, relaxed sandwich structures of the Li_2O_2/Co_3O_4 interface, charge transfer analysis of the up-layer and down-layer of Li_2O_2 in the relaxed sandwich structure of Li_2O_2/Co_3O_4, calculated potential energy profile of the Li_2O decomposition path at the Co_3O_4 (110)B surface, and the structure of the TM-doped Co_3O_4 (111) surface (PDF)

■ AUTHOR INFORMATION

Corresponding Author

*E-mail for J.L.: jliu@mail.sic.ac.cn.

Notes

The authors declare no competing financial interest.

■ ACKNOWLEDGMENTS

This work is financially supported by the One-Hundred-Talent Project of the Chinese Academy of Sciences, and NSFC (51432010).

■ REFERENCES

(1) Girishkumar, G.; McCloskey, B.; Luntz, A. C.; Swanson, S.; Wilcke, W. *J. Phys. Chem. Lett.* **2010**, *1*, 2193−2203.

(2) Cheng, F. Y.; Chen, J. *Chem. Soc. Rev.* **2012**, *41*, 2172−2192.

(3) Shao, Y. Y.; Ding, F.; Xiao, J.; Zhang, J.; Xu, W.; Park, S.; Zhang, J. G.; Wang, Y.; Liu, J. *Adv. Funct. Mater.* **2013**, *23*, 987−1004.

(4) Li, F. J.; Zhang, T.; Zhou, H. S. *Energy Environ. Sci.* **2013**, *6*, 1125−1141.

(5) Peng, Z. Q.; Freunberger, S. A.; Chen, Y. H.; Bruce, P. G. *Science* **2012**, *337*, 563−566.

(6) Jung, H. G.; Hassoun, J.; Park, J. B.; Sun, Y. K.; Scrosati, B. *Nat. Chem.* **2012**, *4*, 579−585.

(7) Christensen, J.; Albertus, P.; Sanchez-Carrera, R. S.; Lohmann, T.; Kozinsky, B.; Liedtke, R.; Ahmed, J.; Kojic, A. *J. Electrochem. Soc.* **2012**, *159*, R1−R30.

(8) Debart, A.; Bao, J.; Armstrong, G.; Bruce, P. G. *J. Power Sources* **2007**, *174*, 1177−1182.

(9) Debart, A.; Paterson, A. J.; Bao, J.; Bruce, P. G. *Angew. Chem., Int. Ed.* **2008**, *47*, 4521−4524.

(10) Read, J. *J. Electrochem. Soc.* **2002**, *149*, A1190−A1195.

(11) Zhang, G. Q.; Zheng, J. P.; Liang, R.; Zhang, C.; Wang, B.; Hendrickson, M.; Plichta, E. J. *J. Electrochem. Soc.* **2010**, *157*, A953−A956.

(12) Cheng, H.; Scott, K. *J. Power Sources* **2010**, *195*, 1370−1374.

(13) Mizuno, F.; Nakanishi, S.; Kotani, Y.; Yokoishi, S.; Iba, H. *Electrochemistry* **2010**, *78*, 403−405.

(14) Débart, A.; Bao, J.; Armstrong, G.; Bruce, P. G. *J. Power Sources* **2007**, *174*, 1177−1182.

(15) Lu, Y. C.; Gasteiger, H. A.; Parent, M. C.; Chiloyan, V.; Shao-Horn, Y. *Electrochem. Solid-State Lett.* **2010**, *13*, A69−A72.

(16) Thapa, A. K.; Saimen, K.; Ishihara, T. *Electrochem. Solid-State Lett.* **2010**, *13*, A165−A167.

(17) Trahey, L.; Johnson, C. S.; Vaughey, J. T.; Kang, S. H.; Hardwick, L. J.; Freunberger, S. A.; Bruce, P. G.; Thackeray, M. M. *Electrochem. Solid-State Lett.* **2011**, *14*, A64−A66.

(18) Lee, J. H.; Black, R.; Popov, G.; Pomerantseva, E.; Nan, F. H.; Botton, G. A.; Nazar, L. F. *Energy Environ. Sci.* **2012**, *5*, 9558−9565.

(19) Jin, L.; Xu, L. P.; Morein, C.; Chen, C. H.; Lai, M.; Dharmarathna, S.; Dobley, A.; Suib, S. L. *Adv. Funct. Mater.* **2010**, *20*, 3373−3382.

(20) Thapa, A. K.; Ishihara, T. *J. Power Sources* **2011**, *196*, 7016−7020.

(21) Wang, L.; Zhao, X.; Lu, Y. H.; Xu, M. W.; Zhang, D. W.; Ruoff, R. S.; Stevenson, K. J.; Goodenough, J. B. *J. Electrochem. Soc.* **2011**, *158*, A1379−A1382.

(22) Lee, J. H.; Black, R.; Popov, G.; Pomerantseva, E.; Nan, F. H.; Botton, G. A.; Nazar, L. F. *Energy Environ. Sci.* **2012**, *5*, 9558−9565.

(23) Cui, Y. M.; Wen, Z. Y.; Liu, Y. *Energy Environ. Sci.* **2011**, *4*, 4727−4734.

(24) Lu, Y. C.; Xu, Z. C.; Gasteiger, H. A.; Chen, S.; Hamad-Schifferli, K.; Shao-Horn, Y. *J. Am. Chem. Soc.* **2010**, *132*, 12170−12171.

(25) Peng, Z.; Freunberger, S. A.; Chen, Y.; Bruce, P. G. *Science* **2012**, *337*, 563−566.

(26) Sun, B.; Munroe, P.; Wang, G. X. *Sci. Rep.* **2013**, DOI: 10.1038/srep02247.

(27) He, P.; Wang, Y. G.; Zhou, H. S. *Chem. Commun.* **2011**, *47*, 10701−10703.

(28) Thotiyl, M. M. O.; Freunberger, S. A.; Peng, Z. Q.; Chen, Y. H.; Liu, Z.; Bruce, P. G. *Nat. Mater.* **2013**, *12*, 1050−1056 DOI: 10.1038/nmat3737.

(29) Shui, J. L.; Karan, N. K.; Balasubramanian, M.; Li, S. Y.; Liu, D. J. *J. Am. Chem. Soc.* **2012**, *134*, 16654−16661.

(30) McCloskey, B. D.; Scheffler, R.; Speidel, A.; Bethune, D. S.; Shelby, R. M.; Luntz, A. C. *J. Am. Chem. Soc.* **2011**, *133*, 18038−18041.

(31) Zhang, L. L.; Wang, Z. L.; Xu, D.; Xu, J. J.; Zhang, X. B.; Wang, L. M. *Chin. Sci. Bull.* **2012**, *57*, 4210−4214.

(32) Zhang, G. Q.; Zheng, J. P.; Liang, R.; Zhang, C.; Wang, B.; Au, M.; Hendrickson, M.; Plichta, E. J. *J. Electrochem. Soc.* **2011**, *158*, A822−A827.

(33) Yang, W.; Salim, J.; Ma, C.; Ma, Z. H.; Sun, C. W.; Li, J. Q.; Chen, L. Q.; Kim, Y. *Electrochem. Commun.* **2013**, *28*, 13−16.

(34) Chen, J.; Selloni, A. *J. Phys. Chem. Lett.* **2012**, *3*, 2808−2814.

(35) Khodakov, A. Y.; Lynch, J.; Bazin, D.; Rebours, B.; Zanier, N.; Moisson, B.; Chaumette, P. *J. Catal.* **1997**, *168*, 16−25.

(36) Xie, X.; Li, Y.; Liu, Z. Q.; Haruta, M.; Shen, W. *Nature* **2009**, *458*, 746−749.
(37) Black, R.; Lee, J. H.; Adams, B.; Mims, C. A.; Nazar, L. F. *Angew. Chem., Int. Ed.* **2013**, *52*, 392−396.
(38) Zhong, L.; Mitchell, R. R.; Liu, Y.; Gallant, B. M.; Thompson, C. V.; Huang, J. Y.; Mao, S. X.; Shao-Horn, Y. *Nano Lett.* **2013**, *13*, 2209−2214.
(39) Mo, Y. F.; Ong, S. P.; Ceder, G. *Phys. Rev. B* **2011**, *84*, 1−9.
(40) Hummelshoj, J. S.; Blomqvist, J.; Datta, S.; Vegge, T.; Rossmeisl, J.; Thygesen, K. S.; Luntz, A. C.; Jacobsen, K. W.; Norskov, J. K. *J. Chem. Phys.* **2010**, *132*, 071101 DOI: 10.1063/1.3298994.
(41) Hummelshoj, J. S.; Luntz, A. C.; Norskov, J. K. *J. Chem. Phys.* **2013**, *138*, 1−12.
(42) Kresse, G.; Furthmüller, J. *Phys. Rev. B* **1996**, *54*, 11169−11186.
(43) Kresse, G.; Furthmüller, J. *Comput. Mater. Sci.* **1996**, *6*, 15−50.
(44) Xu, X.-L.; Chen, Z.-H.; Li, Y.; Chen, W.-K.; Li, J.-Q. *Surf. Sci.* **2009**, *603*, 653−658.
(45) Jiang, D.-e.; Dai, S. *Phys. Chem. Chem. Phys.* **2011**, *13*, 978−984.
(46) Dudarev, S. L.; Botton, G. A.; Savrasov, S. Y.; Humphreys, C. J.; Sutton, A. P. *Phys. Rev. B* **1998**, *57*, 1505−1509.
(47) Ren, Y.; Ma, Z.; Qian, L. P.; Dai, S.; He, H. Y.; Bruce, P. G. *Catal. Lett.* **2009**, *131*, 146−154.
(48) Razdobarov, V. A.; Sadykov, V. A.; Veniaminov, S. A.; Bulgakov, N. N.; Kovalenko, O. N.; Pankratiev, Y. D.; Popovskii, V. V.; Kryukova, G. N.; Tikhov, S. F. *React. Kinet. Catal. Lett.* **1988**, *37*, 109−114.
(49) Pollard, M. J.; Weinstock, B. A.; Bitterwolf, T. E.; Griffiths, P. R.; Newbery, A. P.; Paine, J. B., III *J. Catal.* **2008**, *254*, 218−225.
(50) Petitto, S. C.; Langell, M. A. *J. Vac Sci. Technol. A* **2004**, *22*, 1690−1696.
(51) Radin, M. D.; Rodriguez, J. F.; Tian, F.; Siegel, D. J. *J. Am. Chem. Soc.* **2012**, *134*, 1093−1103.
(52) Chase, M. W. *NIST-JANAF Thermochemical Tables*, 4th ed.; American Institute of Physics: Melville, NY, 1998.
(53) Chase, M. W. American Institute of Physics: Melville, NY, 1998.
(54) Rossmeisl, J.; Norskov, J. K.; Taylor, C. D.; Janik, M. J.; Neurock, M. *J. Phys. Chem. B* **2006**, *110*, 21833−21839.
(55) Xu, X.-L.; Yang, E.; Li, J.-Q.; Li, Y.; Chen, W.-K. *ChemCatChem.* **2009**, *1*, 384−392.
(56) Kapteijn, F.; Rodriguez-Mirasol, J.; Moulijn, J. A. *Appl. Catal., B* **1996**, *9*, 25−64.
(57) Xu, R.; Zeng, H. C. *J. Phys. Chem. B* **2003**, *107*, 926−930.
(58) Liu, X. H.; Qiu, G. Z.; Li, X. G. *Nanotechnology* **2005**, *16*, 3035−3040.
(59) Yeo, B. S.; Bell, A. T. *J. Am. Chem. Soc.* **2011**, *133*, 5587−5593.
(60) Esswein, A. J.; McMurdo, M. J.; Ross, P. N.; Bell, A. T.; Tilley, T. D. *J. Phys. Chem. C* **2009**, *113*, 15068−15072.
(61) Lu, B. A.; Cao, D. X.; Wang, P.; Wang, G. L.; Gao, Y. Y. *Int. J. Hydrogen Energy* **2011**, *36*, 72−78.
(62) Mitchell, R. R.; Gallant, B. M.; Shao-Horn, Y.; Thompson, C. V. *J. Phys. Chem. Lett.* **2013**, *4*, 1060−1064.
(63) Gallant, B. M.; Kwabi, D. G.; Mitchell, R. R.; Zhou, J.; Thompson, C. V.; Shao-Horn, Y. *Energy Environ. Sci.* **2013**, *6*, 2518−2528.
(64) Ren, X.; Zhu, J.; F, D.; Liu, J.; Zhang, W. *J. Phys. Chem. C* **2014**, *118*, 22412−22418.
(65) Pal, R.; Wang, L. M.; Pei, Y.; Wang, L. S.; Zeng, X. C. *J. Am. Chem. Soc.* **2012**, *134*, 9438−9445.
(66) Freunberger, S. A.; Chen, Y. H.; Drewett, N. E.; Hardwick, L. J.; Barde, F.; Bruce, P. G. *Angew. Chem., Int. Ed.* **2011**, *50*, 8609−8613.
(67) Zhang, L. L.; Zhang, X. B.; Wang, Z. L.; Xu, J. J.; Xu, D.; Wang, L. M. *Chem. Commun.* **2012**, *48*, 7598−7600.
(68) Lim, H. D.; Park, K. Y.; Gwon, H.; Hong, J.; Kim, H.; Kang, K. *Chem. Commun.* **2012**, *48*, 8374−8376.
(69) Zhang, K. J.; Zhang, L. X.; Chen, X.; He, X.; Wang, X. G.; Dong, S. M.; Han, P. X.; Zhang, C. J.; Wang, S.; Gu, L.; Cui, G. L. *J. Phys. Chem. C* **2013**, *117*, 858−865.
(70) Nakamura, R.; Nakato, Y. *J. Am. Chem. Soc.* **2004**, *126*, 1290−1298.
(71) McFarland, E. W.; Metiu, H. *Chem. Rev.* **2013**, *113*, 4391−4427.
(72) Metiu, H.; Chrétien, S.; Hu, Z.; Li, B.; Sun, X. *J. Phys. Chem. C* **2012**, *116*, 10439−10450.
(73) Gallant, B. M.; Kwabi, D. G.; Mitchell, R. R.; Zhou, J. G.; Thompson, C. V.; Shao-Horn, Y. *Energy Environ. Sci.* **2013**, *6*, 2518−2528.
(74) Lu, Y. C.; Shao-Horn, Y. *J. Phys. Chem. Lett.* **2013**, *4*, 93−99.
(75) McCloskey, B. D.; Scheffler, R.; Speidel, A.; Girishkumar, G.; Luntz, A. C. *J. Phys. Chem. C* **2012**, *116*, 23897−23905.
(76) Cui, Y. M.; Wen, Z. Y.; Liang, X.; Lu, Y.; Jin, J.; Wu, M. F.; Wu, X. W. *Energy Environ. Sci.* **2012**, *5*, 7893−7897.